Int J Adv Manuf Technol (2012) 60:1009–1015
DOI 10.1007/s00170-011-3664-0

ORIGINAL ARTICLE

Study on direct fabrication of ceramic shell mold with slurry-based ceramic laser fusion and ceramic laser sintering

Hsiao Chuan Yen · Hwa Hsing Tang

Received: 15 April 2011 / Accepted: 20 September 2011 / Published online: 12 October 2011

Abstract Through studying the porosity of the ceramic parts fabricated with slurry-based rapid prototyping process of ceramic laser fusion and ceramic laser sintering, the feasibility of directly fabricating ceramic shell mold was investigated in this paper. Although the total porosity of the fusion part was low, microcracks led to low strength, which was hardly enhanced by post-treatment of infiltration. On the other hand, by adjusting the slurry formulation and varying the laser scanning energy, the open porosity of the sintered part was over 90 vol.% of the total porosity. High open porosity resulted in good permeability, which is one of the important characteristics of the ceramic shell mold for investment casting. To verify the feasibility of producing casting part with ceramic shell molds fabricated by the processes of ceramic laser fusion and ceramic laser sintering, the casting process was conducted to obtain the casting parts.

Keywords Rapid prototyping · Ceramic laser fusion · Ceramic laser sintering · Permeability · Porosity · Ceramic shell mold

1 Introduction

Rapid prototyping is a nontraditional technology based on layer manufacturing. Because of the increasing demand of producing ceramic and metal parts, researches have switched to investigate the feasibility of fabricating ceramic and metal components instead of polymer parts. A variety of techniques has been studied, such as stereolighography, selective laser sintering (SLS), laminated object manufacturing, fused deposition modeling, and 3D printing. Some researches regarding the fabrication of ceramic shell mold with technique of layer manufacturing were reported. Klocke and Ader [1] studied the laser sintering of investment casting shells and cores to cast metal prototypes; Tang et al. [2] studied the feasibility of using silica sand and process of SLS to build casting molds for metal casting; Zhou et al. [3] directly fabricated an integral ceramic mold by stereolithography; Bassoli et al. [4] verified the feasibility and evaluated the dimensional accuracy of 3D printing technique applied to rapid casting.

Tang [5, 6] invented two slurry-based rapid prototyping processes, ceramic laser fusion (CLF) and ceramic laser sintering (CLS), in 2001 and 2007, respectively. Both processes are somewhat similar to SLS in the principle of using laser scanning to fabricate parts, but use slurry, which was composed of a structural material (high melting point ceramic powder) and an inorganic binder (low melting point ceramic powder). The advantage of the slurry-based process is the capability of casting ultra-thin layer, which leads to higher green density and better surface of the green part [6]. CLF and CLS have identical processes shown in Fig. 1 but employs different energy density generated by laser irradiation.

In CLF, because the working temperature induced from the laser scanning is higher than the melting point of the structural material, the structural material melts; the consolidation mechanism is called “fusion”. On the other hand, the working temperature of CLS is lower than the melting point of the structural material but is higher than that of the inorganic binder. Consequently, the structural material remains in the solid phase while the liquefied

H. C. Yen
Department of Mechanical Engineering,
National Taipei University of Technology,
Taipei, Taiwan

H. H. Tang (✉)
Graduate Institute of Manufacturing Technology,
National Taipei University of Technology,
No. 1, Chung Hsiao East Road, Sec. 3,
Taipei 10608, Taiwan
e-mail: tanghwahsing@gmail.com

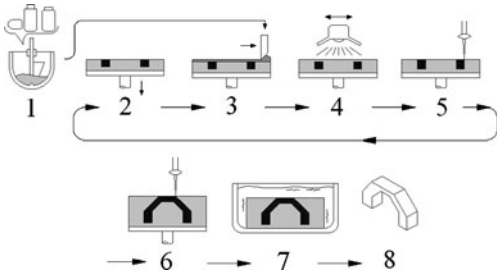

Fig. 1 Schematic of the process of CLF/CLS *1* making slurry, *2* descending platform for one layer thickness, *3* casting a thin slurry layer by a moving scraper, *4* drying the slurry with a heater to solidify the surface to be a smooth green layer, *5* selectively scanning the green layer with a CO_2 laser, *6* repeating steps *2*–*5* to form a 3D green part, *7* removing the unscanned green portion, *8* completing the green part

inorganic binder is almost instantaneously driven by intense capillary forces to fill up the space between the solid particles; the consolidation mechanism is called "partial melting" or "liquid phase sintering" (LPS) [7], which is defined as "sintering" in this paper.

By observing the porosity, this paper aims to investigate the feasibility of producing casting parts through a ceramic shell mold made by CLF/CLS. The porosity is correlated with the air escaping, which is preferentially considered in ceramic shell mold, during the casting process.

2 Experimental procedure

The experiment included four steps. Firstly, to achieve a reliable consolidation of the particles, the line overlap and planar overlap should be over 50%. Therefore, obtaining the scanning line width (W_L) and depth (D_L) in advance is a must. Secondly, fusion specimens and sintering specimens were fabricated for investigating their characteristics. Thirdly, porosity of each specimen was observed. Eventually, ceramic shell molds were fabricated by CLF/CLS to verify the feasibility of manufacturing casting parts.

2.1 Materials

The slurry was composed of SiO_2 powder (melting point ~1,750°C, Chin Ching Silica Sand, Taiwan) as a structure material, silica sol (melting point ~1,700°C, Nissan Chemical SNOWTEX® ST-40, Japan) as an inorganic binder, volcanic clay (melting point ~1,200°C, Wyoming Bentonite clay, USA) as a suspending agent, and deionized water as a solvent.

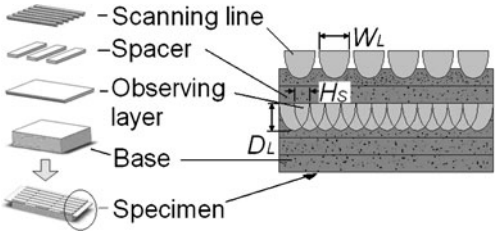

Fig. 2 Schematic of a specimen for measuring scanning line width and depth

Table 1 shows different compositions of the slurry. Slurry A, which contains the lowest silica sol content, was employed to fabricate green fusion specimens. For observing the influence of the binder content on porosity, slurries B and C were used to fabricate green sintering specimens. Slurry B, however, contained more binders than slurry C did.

The variety of the composition will influence the characteristics of the slurry. High silica sol content leads to rapid sedimentation. At a relatively low water content of less than 10 wt.%, the clay performs the role of a binder, holding itself and other particles together. Clay thus becomes the essential ingredient in forming ceramic powder at low water content. At a high water content (in excess of 50 wt.%), the clay performs the role of the suspending agent and is added to other ceramic materials in order to help them in suspension during forming from slurries [8]. Because of higher silica sol content in slurry B, it should have more clay than slurry C does to prevent sedimentation.

2.2 Scanning line width and depth

The feasibility of fabricating the ceramic parts with the laser-based process depends on the energy density irradiated on the layer surface. The energy density can be represented by Eq. 1.

$$E = \frac{P_L}{V_S \times H_S} \tag{1}$$

Here

E Energy density on surface (J/mm^2)
P_L Laser average power (W)

Table 1 The composition of the slurry for fabricating ceramic specimens

Green specimen	Slurry	Composition			
		SiO_2 (g)	Clay (g)	Silica sol (g)	Deionized water (g)
Fusion specimen	Slurry A	100	7	3	80
Sintering specimen	Slurry B	100	7	9	80
	Slurry C	100	3	7	80

Table 2 Scanning parameter combination for fabrication of sintering specimens

Slurry	P_L (W)	V_S (mm/s)	H_S (mm)	Layer thickness (μm)
Slurry B	14	500	0.12	20
Slurry C	10	370	0.12	20
	8	200	0.12	20

V_S Laser scanning speed (mm/s)
H_S Hatch space (mm)

Selecting a high energy density laser scanning to achieve a consolidation mechanism of full melting is the principle of building a fusion part, while the consolidation mechanism of a sintering part is based on the LPS, which is induced with a suitable energy density. Yen et al. [9] investigates laser scanning parameters on the fabrication of ceramic parts by LPS. The hatch space (H_S) is based on the overlap of W_L and the layer thickness is based on the overlap of D_L, respectively. Figure 2 illustrates the schematic of the specimen for observing W_L and D_L. W_L and D_L were measured by an optical microscope equipped with an *X-Y* platform. For a specific hatch space, scanning energy density was varied with laser power and scanning speed. The consolidation mechanism was verified by observing the topography with a scanning electron microscope.

Firstly, high energy density was employed to fabricate the base and the spacer of the specimen. Secondly, a single observing fusion layer was built with slurry A and a specified scanning parameter combination (P_L=19 W, V_S=60 mm/s and H_S=0.1 mm) for obtaining D_L. A single layer with a thickness of 40 μm was then casted and scanned without overlap for achieving W_L. Afterwards, the same process was repeated with slurry C and specified scanning parameter combinations listed in Table 2 to build sintering layer and to obtain D_L. A single layer with a thickness of 20 μm was then casted and scanned without overlap for achieving W_L.

2.3 Fabricating green fusion specimens by ceramic laser fusion

Based on the W_L and D_L obtained from the specimens, the green fusion specimen (10×10×1 mm), made for observing characteristics, was fabricated with slurry A (layer thickness of 40 μm, and scanning parameter combination P_L= 19 W, V_S=60 mm/s, and H_S=0.1 mm).

2.4 Fabricating green sintering specimens by ceramic laser sintering

Based on the W_L and D_L obtained from the specimens, the green sintering specimen (10×10×1 mm), made for observing characteristics, were fabricated with slurries B and C (layer thickness of 20 μm, and the scanning parameter combination listed in Table 2).

2.5 Porosity measurement

An electronic densimeter (ALFA Mirage Co., Ltd., Osaka, Japan, Model: SD-120 L) was used to figure out the total volume of the part (V_{all}). A porosity measurement was conducted by infiltrating liquefied wax into the open pores with capillary force. Equations 2, 3, 4, 5, 6, and 7 were used to individually figure out bulk density, open porosity, and closed porosity of the part. "*A*" represents the weight of the laser sintering part, which was measured after cooling at room temperature for an hour. The part was then immersed in the 70°C liquefied wax for 30 min and taken out for cooling at room temperature for another 30 min. "*B*" represents the weight of the infiltrated part. "*C*" represents the weight of the infiltrated part when it was immersed in a tank filled up with 25°C water. The theoretical density of SiO_2 and wax are 2.7 and 0.9 g/cm^3, respectively.

$$V_{\text{all}} = (B - C)/D_{\text{water}} \tag{2}$$

$$V_o = (B - A)/D_{\text{wax}} \tag{3}$$

$$V_c = V_{\text{all}} - V_o - (A/D_{\text{silica}}) \tag{4}$$

$$\text{Bulk density} = A/(V_{\text{all}} - V_o) \tag{5}$$

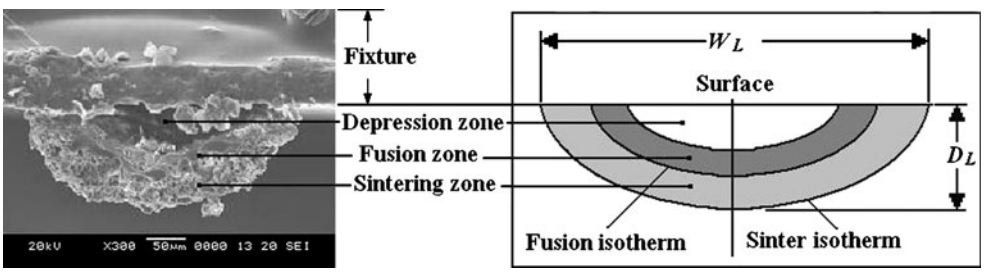

Fig. 3 Temperature distribution corresponding to the energy distribution of Gaussian beam

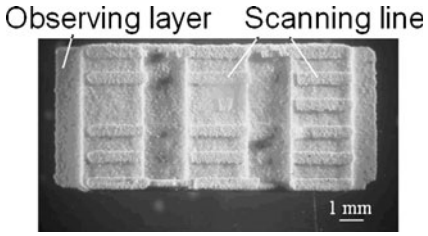

Fig. 4 Specimen for measuring scanning line depth and width

$$\text{Open porosity}(\%) = (V_o/V_{\text{all}})\bullet 100 \quad (6)$$

$$\text{Closed porosity}(\%) = (V_c/V_{\text{all}})\bullet 100 \quad (7)$$

where, V_{all} is the total volume of the part; V_o is the total volume of the open pores; V_c is the total volume of the closed pores; and D is density.

2.6 Manufacturing casting parts with a ceramic shell mold

To verify the feasibility of producing casting parts, the casting parts were manufactured by using ceramic shell molds fabricated through CLF and CLS, respectively.

3 Results and discussion

3.1 Scanning line width and depth

Apparently, the higher the laser power, the higher the energy density; the higher the scanning speed, the lower the energy; the larger the hatch space, the lower the energy density. High-energy density will lead to the melting of all ceramic particles, but low-energy density will induce a consolidation mechanism of LPS to bind the ceramic particles.

Green specimens were fabricated using a homemade apparatus equipped with a 20 W CO_2 laser [10]. Laser energy was absorbed and transferred from the surface to the interior. Figure 3 schematically shows a temperature distribution corresponding to the energy distribution of the Gaussian beam, which has the maximum energy intensity at the beam midpoint.

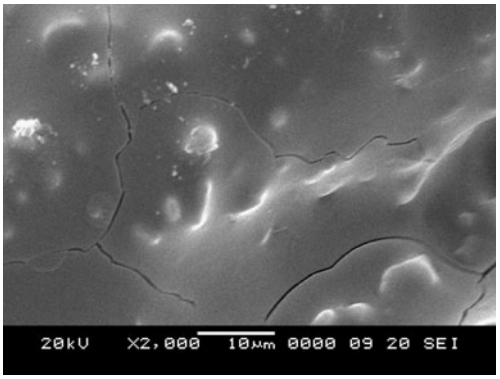

Fig. 6 Microcracks in the fusion part

Under the condition of constant scanning speed and beam size, the temperature of the scanned surface will reach the melting point of the clay (~1,200°C) as the laser power is raised to a certain value. The melted clay binds the solid silica particles to form a liquid phase sintering zone. If the laser power continuously increases, the silica particles on the surface will melt and the fusion zone with extend from the surface to the interior. Eventually, a depression zone (melting pool) is formed. The area beneath the fusion zone is the sintering zone. The property transformation zone (scanned region), which includes the fusion zone and sintering zone, can be taken apart from the green block after the green region (unscanned region) is removed. D_L is proportional to the amount of energy delivered to the green layer. In other words, a higher laser power or a lower scanning speed enlarges D_L. If the layer thickness is smaller than D_L, the fusion zone of each layer overlaps, the fusion part, can then be manufactured. The specimen shown in Fig. 4 was one of the specimens, which were employed to measure D_L and W_L. The average W_L=0.5 mm and D_L= 0.2 mm were achieved individually from fusion layers. The average W_L=0.47 mm and D_L=0.045 mm were obtained individually from sintering layers.

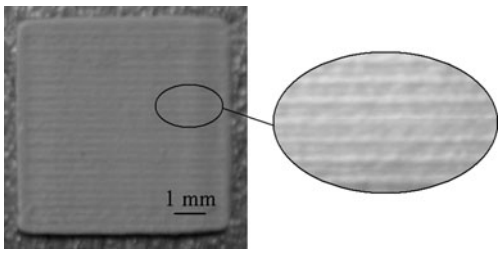

Fig. 5 Specimen (10×10×1 mm) fabricated by the process of ceramic laser fusion

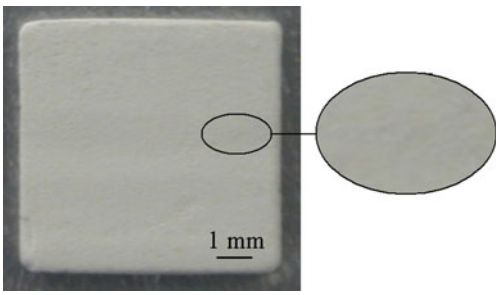

Fig. 7 Specimen (10×10×1 mm) fabricated by the process of ceramic laser sintering

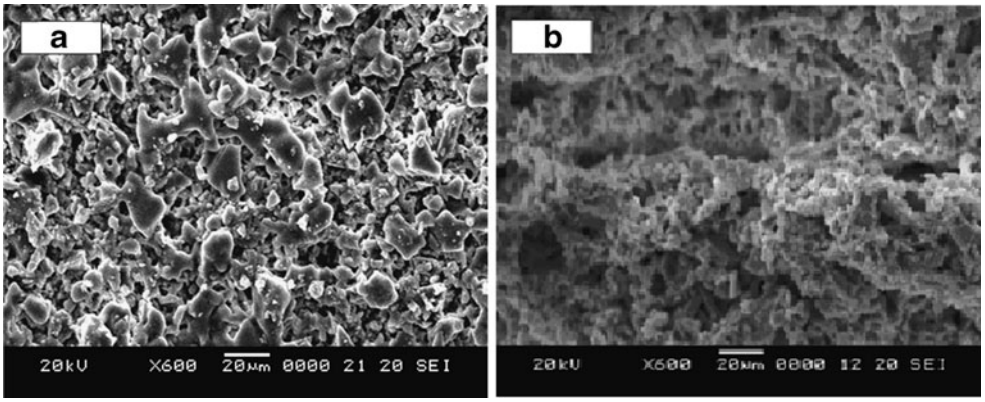

Fig. 8 **a** Surface of the specimen built with laser power of 14 W. **b** Fracture surface micrograph of the specimen built with laser power of 14 W

3.2 The characteristics of green fusion specimen

Based on W_L=0.5 mm and D_L=0.2 mm, the specimen shown in Fig. 5 was fabricated with consolidation mechanism of fusion. The poor surface, which was induced by the depressions along the scanning direction, was observed. The interior of the fusion specimen contained many closed pores. Moreover, microcracks (Fig. 6) were observed. The closed pores were unfavorable to the escaping of air during the metal casting; therefore, no further observation of the porosity of the fusion specimen was conducted.

Theoretically, the fusion part possesses high density, which results in high mechanical strength. The high density resulted from the full melting ceramic powder. But large numbers of microcracks, which quite evenly distributed throughout the specimen and deteriorated the strength of the fusion specimen, were observed. As the ceramic is a kind of brittle material, which hardly deforms plastically and its tensile strength is only one tenth of its compressive strength; therefore, thermal stress easily induces microcracks. In the current investigation, a high-laser power with a low-scanning speed was employed to achieve full melting. Because of the successive scanning, the surface temperature increased rapidly; therefore, the thermal expansion on the surface was larger than that at the interior of the specimen. The surface and the interior of the specimen bore compressive stress and tensile stress, respectively. After laser scanning, the scanned surface came into contact with the cold air in the atmosphere; therefore, the cooling speed on the surface was faster than that in the interior. Such phenomenon generated creak formation during the manufacturing process. Obviously, high density, rough surface, microcracks, and closed pores were the characteristics of the ceramic fusion specimen.

3.3 The characteristics of the green sintering specimen

Based on W_L=0.47 mm and D_L=0.045 mm, the specimen shown in Fig. 7 was fabricated with consolidation mechanism of sintering.

Figure 8a and b demonstrate the surface and fracture surface micrograph of the CLS specimen built with laser power of 14 W. Figure 8a shows that consolidation mechanism of sintering appeared on the surface. Although partial melting occurred locally, the individual molten areas were less than 20×20 μm and did not connect to each other. Figure 8b reveals a porous structure; no extensive melting area, which prohibited the connection of the pores existing between the layers. The porous green sintering specimens could also be fabricated with the slurry C, which contained fewer binders as aforementioned in Section 2.1.

3.4 Porosity of the green sintering specimens

Table 3 shows porosity of the green specimens fabricated with different laser powers and with two kinds of slurry

Table 3 The porosity of the specimens fabricated with different laser powers and with different slurries listed in Table 1

Green specimen	material	Laser power (W)	Porosity (vol%)		
			Open	Closed	Total
A	Slurry B	14	30.0	16.0	46.0
B	Slurry C	10	38.0	7.8	45.8
		10	40.6[a]	5.2[a]	45.8[a]
C		8	37.0	7.4	44.4
		8	42.5[a]	4.1[a]	46.6[a]

[a]After post-sintering in a furnace

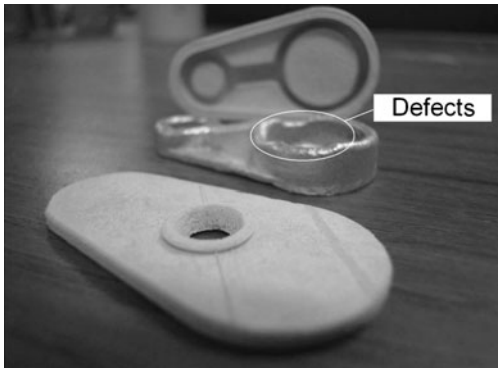

Fig. 9 Defects on a metal part made by a ceramic shell mold fabricated with the process of CLF

mentioned in Section 2.1. Apparently, the difference of total porosity (open porosity + closed porosity) was very small. The total porosity of the green specimen A made of slurry B, in which more binders were contained, was 46 vol.%. The closed porosity of green specimen A was higher than that of the green specimens B and C. One of the reasons was that the higher laser power led to more molten clay which blocked a part of the pores to form closed pores during the process of binder melting. The highest density of green specimen A was only 84% after infiltrating a low melting point material.

For the green specimens made of slurry C, a minor adjustment of the laser power did not lead to an obvious variation of the total porosity. The total porosity was almost the same as the porosity of the green specimen A; however, the closed porosity of the green specimen made of slurry C reduced to 7.4~7.8 vol.% but the open porosity increased to 37~38 vol.%. When a low melting point material infiltrated into the green sintering specimen, the density increased to around 92%. Furthermore, when a green sintering specimen was placed in a furnace with a constant temperature of 1,150°C for 2 h to be a sintered ceramic part, the total porosity of the sintered part was almost unchanged, but the closed porosity was reduced around 3 vol.% while the open porosity increased to 40.6~42.5 vol.%. Due to the increase of open porosity, the density of the sintered part was increased to 95% after infiltration. The microstructure of high open porosity can also be verified with Fig. 8.

3.5 Casting parts fabrication

An aluminum part shown in Fig. 9 was built with a ceramic shell mold fabricated by the process of CLF. Defects were due to high closed porosity, which caused difficulty of air exhaust during casting. The inner surface of the ceramic shell mold significantly influenced the roughness of casting part; therefore, a good inner surface is a must, and is in favor of mold for investment casting. On account of the porous structure of the sintering part, the air trapped in the pores escapes easily during the casting; such character is preferred in ceramic shell mold. Figure 10 shows a casting waterwheel successfully made by a ceramic shell mold fabricated with the process of CLS. The surface roughness of the waterwheel was 3.07~4.67 μm (Ra).

4 Conclusion

According to the aforementioned characteristics of the fusion parts and the sintering parts, we can evaluate the feasibility of applying these two consolidation mechanisms for producing parts with desired mechanical strength or porosity.

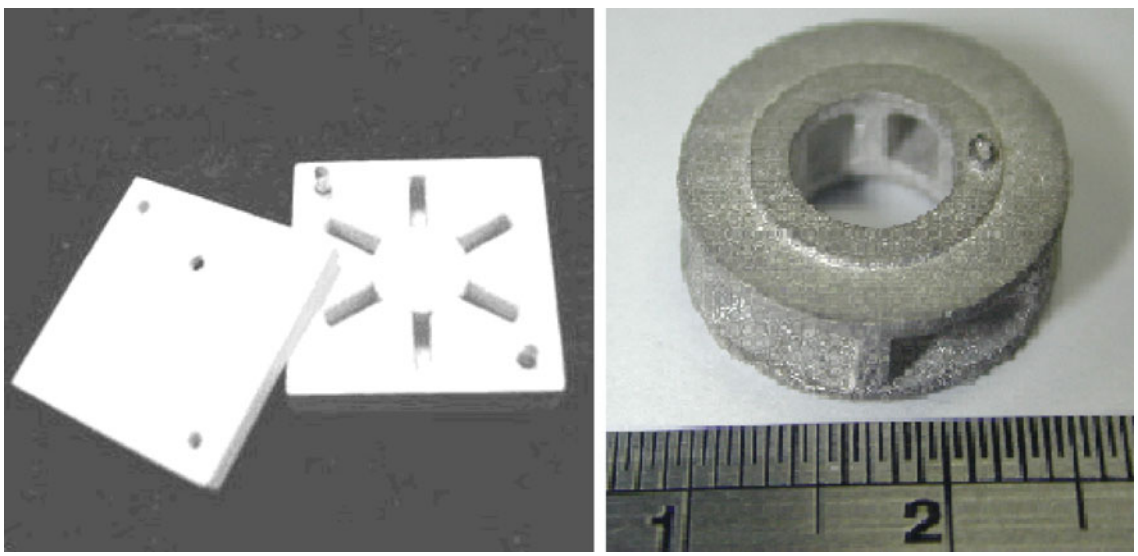

Fig. 10 A casting waterwheel made by a ceramic shell mold fabricated with the process of CLS

In comparison with CLS, CLF can lead to reducing porosity and achieving higher density. Because silica is a brittle material, high-energy laser scanning easily induces thermal cracks; such cracking might cause a minor defect to become a destructive crack development. Because a great portion of the closed pores in the fusion structure, the molten material cannot infiltrate into the closed pores to improve density and to enhance the mechanical strength of the part. Obviously, CLF is not suitable for parts that need high permeability or high strength. On the other hand, a part with high porosity can be built with CLS. By changing the slurry formulation and varying the delivering energy, the open porosity can be adjusted. As a result, the total porosity of a sintering part can be greater than 45 vol.% and the open porosity can be greater than 90 vol.% of the total porosity. However, lower level consolidation (higher residual porosity) will not reach a higher strength. After infiltrating a high strength material, the density can be increased to 95%, which will improve mechanical strength. Because of the high open porosity of the sintering part, CLS is feasible and promising for manufacturing ceramic shell mold, which needs high permeability.

Due to the difficulty of modifying characteristics of the fusion parts, our future work will concentrate on CLS to fabricate ceramic parts, which demand high permeability, such as ceramic filter and porous scaffold designs for tissue engineering.

Acknowledgments This work was supported by National Science Council of ROC [grant number NSC96-2221-E-027-103-MY2] and Ministry of Education, ROC. The authors wish to greatly thank Mr. Jin Hau Jou for the porosity measurements and the molds making.

References

1. Klocke F, Ader C (2003) Direct laser sintering of ceramics. In: Proceeding of the 14th SFF Symp. Univ. of Texas at Austin, USA, pp. 447–455
2. Tang Y, Fuh JYH, Loh HT, Wong YS, Lu L (2003) Direct laser sintering of a silica sand. Mater Design 24:623–629
3. Zhou WZ, Li D, Chen ZW, Chen S (2010) Direct fabrication of an integral ceramic mould by stereolithography. Proc IMechE Part B: J Eng Manuf 224:237–243
4. Bassoli E, Gatto A, Iuliano L, Violante MG (2007) 3D printing technique applied to rapid casting. Rapid Prototyping J 13:148–155
5. Tang HH (2001) Method for rapid forming of a ceramic work piece. U.S. patent no. 6,217,816
6. Tang HH (2006) Building ultra-thin layers by ceramic laser sintering. Mater Trans, J Jpn Inst Met 47:889–897
7. Kruth J-P, Levy G, Klocke F, Childs THC (2007) Consolidation phenomena in laser and powder-bed based layered manufacturing. Annals of the CIRP 56:730–759
8. Phillips GC (1991) A concise introduction to ceramic. Van Nostrand Reinhold, New York
9. Yen HC, Chiu ML, Tang HH (2009) Laser scanning parameters on fabrication of ceramic parts by liquid phase sintering. J Eur Ceram Soc 29:1331–1336
10. Yen HC, Tang HH (2008) Developing a paving system for fabricating ultra-thin layers. Int J Adv Manuf Technol 36:280–287